

# Giant Impurity Effects on Charge Loop Current Order States in Kagome Metals

Seigo Nakazawa<sup>1</sup>, Rina Tazai<sup>2</sup>, Youichi Yamakawa<sup>1</sup>, Seiichiro Onari<sup>1</sup>, and Hiroshi Kontani<sup>1</sup>

<sup>1</sup>*Department of Physics, Nagoya University, Furo-cho, Nagoya 464-8602, Japan*

<sup>2</sup>*Yukawa Institute for Theoretical Physics, Kyoto University, Kyoto 606-8502, Japan.*

(Dated: May 21, 2024)

The exotic electronic states in the charge loop current (cLC) phase, in which the permanent charge current breaks the time-reversal-symmetry (TRS), have been attracting increasing attention in recently discovered kagome metal  $AV_3Sb_5$  ( $A = Cs, Rb, K$ ). Interestingly, the cLC state is sensitively controlled by applying small magnetic field as well as tiny uniaxial strain. In addition, many experiments indicate that the cLC state is extremely sensitive to the small number of impurities. To understand the impurity effects on the cLC electronic states accurately, we analyze the giant unit-cell (up to 300 sites) kagome lattice model with single impurity potential. The loop current is found to be strongly suppressed within the current correlation length  $\xi_J$  centered on the impurity site, where  $\xi_J$  is inversely proportional to the cLC order parameter  $\eta$ . (The cLC order is the pure imaginary hopping integral modulation  $\delta t_{i,j} = \pm i\eta$ .) In addition, both the uniform orbital magnetization  $M_{orb}$  and the anomalous Hall conductivity  $\sigma_{xy}$  are drastically suppressed by dilute impurities. Especially, the suppression ratio  $R = -\Delta M_{orb}/M_{orb}^0$  can exceed 50% by introducing  $\sim 1\%$  impurities. Unexpectedly, the ratio  $R$  is insensitive to  $\eta$ , in highly contrast to a naive expectation that  $R$  is proportional to the current suppression area  $\pi\xi_J^2$ . The obtained giant impurity effect of  $M_{orb}$  would originate from the non-local contribution from the itinerant circulation of electrons. The present study gives a natural explanation why the cLC electronic states in kagome metals are extremely sensitive to the dilute impurities.

## I. INTRODUCTION

Recent years, various quantum phase transitions have been reported in strongly correlated electron systems. Among them, kagome metal  $AV_3Sb_5$  ( $A = Cs, Rb, K$ ) [1, 2] has various interesting phases such as the charge density wave (CDW) [3–6], the nematic state [4, 7–10], and the superconductivity [11, 12]. Thus, it has attracted more attention. The CDW is originated from the  $2 \times 2$  Star-of-David or Tri-Hexagonal bond order (BO) [10]. Significantly, the time-reversal-symmetry (TRS) breaking phase without any spin polarization is reported by the  $\mu$ SR [13–16], the NMR [17], the STM [18], the Kerr effect [19, 20], and the observation of the anomalous Hall conductivity [21–23]. Especially, recent magnetic torque measurement [9] and the electronic magneto-chiral anisotropy (emChA) [24] have presented very convincing evidence for the TRS breaking phase, although its onset temperature,  $T_{cLC}$  is still under debate. Interestingly, Ref. [25] has recently reported that  $T_{cLC} \approx 0$  in an ideal strain-free system, while  $T_{cLC}$  drastically increases under the weak magnetic fields or tiny strains. Consistently, it is theoretically found that the TRS breaking state is sensitively controlled by applying small magnetic field as well as tiny uniaxial strain [26].

The permanent charge loop current (cLC) state without any spin polarization is a natural candidate for the origin of the TRS breaking phase [27, 28]. The cLC order is the “pure imaginary” modulation in the hopping integral,  $\delta t^C = \pm i\eta$ , whereas the BO with the TRS preserving is the “real” one,  $\delta t^B = \pm\phi$  [10, 27, 29–33]. Theoretically, the cLC is induced by the BO fluctuation [34] in kagome metals. The actual current distribution  $J$  in real space is not simply proportional to the cLC order

parameter  $\eta$ , as discussed in Ref. [35]. Therefore,  $J$  is needed to be calculated microscopically. In the triple- $\mathbf{Q}$  cLC state, where the current flows in all three directions in the two-dimensional model, the global TRS is broken and therefore the chirality ( $\chi_{ch} = \pm 1$ ) is well-defined. ( $\chi_{ch}$  changes its sign under the time-reversal operation, while  $\chi_{ch}$  is unchanged under the translational and rotational shifts.) Therefore, the triple- $\mathbf{Q}$  cLC order causes the finite uniform orbital magnetization  $M_{orb}$  [26, 27]. On the other hand, the single- $\mathbf{Q}$  cLC order breaks the local TRS, but it preserves the global TRS. Thus, the uniform  $M_{orb}$  vanishes in the single- $\mathbf{Q}$  cLC order.

In kagome metal  $AV_3Sb_5$  ( $A = Cs, Rb, K$ ), the exotic electronic states in the cLC phase, in which the permanent charge current breaks the TRS, have been attracting increasing attention. Interestingly, the cLC state is sensitively controlled by applying small magnetic field as well as tiny uniaxial strain [25, 26]. In addition, many experiments indicate that the cLC state is extremely sensitive to the small number of impurities. Thus, it is important to study the impurity effect in the cLC order of kagome metals, while its systematic understanding has not been achieved.

In this paper, we analyze the giant unit-cell (up to 300 sites) kagome lattice model with single impurity potential to understand the impurity effects on the cLC electronic states accurately. The loop current is found to be strongly suppressed within the current correlation length  $\xi_J$  centered on the impurity site, where  $\xi_J$  is inversely proportional to the cLC order parameter  $\eta$ . In addition, both the uniform orbital magnetization  $M_{orb}$  and the anomalous Hall conductivity  $\sigma_{xy}$  are drastically suppressed by dilute impurities. Especially, the suppression ratio  $R = -\Delta M_{orb}/M_{orb}^0$  can exceed 50% by introducing  $\sim 1\%$  impurities. Unexpectedly, the ratio  $R$  is insensi-

tive to  $\eta$ , in highly contrast to a naive expectation that  $R$  is proportional to the current suppression area  $\pi\xi_j^2$  that decreases with  $|\eta|$ . The obtained giant impurity effect of  $M_{\text{orb}}$  would originate from the non-local contribution from the itinerant circulation of electrons. The present study gives a natural explanation why the cLC electronic states in kagome metals are extremely sensitive to the dilute impurities.

The microscopic mechanism of the exotic multiple quantum phase transitions has been studied very actively. The mean-field theories as well as the renormalization group theories based on the (extended) Hubbard models have been performed in Refs. [10, 27, 31, 32, 34, 36, 37]. The present authors discovered that the Star-of-David BO state is driven by the paramagnon-interference (PMI) mechanism [10], which is described by the Aslamazov-Larkin vertex corrections that are dropped in the mean-field level approximations. Importantly, the BO fluctuations mediate not only  $s$ -wave or  $p$ -wave superconductivity but also the TRS breaking cLC order [10, 34].

## II. GIANT UNIT-CELL MODEL

First, we introduce the kagome-lattice tight-binding model [10, 37] shown in Fig. 1 (a). The original unit-cell is composed of three sublattices A, B, and C. We put the nearest-neighbor hopping integral  $t = -0.5$  eV. In addition, we introduce the nearest intra-sublattice hopping integral  $t' = -0.02$  eV to prevent the perfect nesting and set the temperature  $T = 0.01$  eV. Hereafter, the unit of energy is eV. Figures 1 (b) and (c) show the band structure and the Fermi surface at the van-Hove singularity (vHS) filling, respectively, where the vHS energy coincides with the chemical potential  $\mu$ . In Fig. 1 (b), the chemical potential is  $\mu = 0$ . The vHS filling in the present model is given by the particle number  $n = n_{\text{vHS}} = 2.55$  per 3 site unit-cell, where the vHS appears at the M point. In Fig. 1 (c), the red, blue, and green points denote the contribution to the Fermi surface from the sublattices A, B, and C, respectively. The present model provides the pure type Fermi surface [3, 38–41]. We focus on the  $b_{3g}$ -orbital of the V ion in the present study. Other  $d$  orbitals also form the large Fermi surface near the vHS energy, which are found to be qualitatively important to understand large  $M_{\text{orb}}$  in kagome metals [26].

The cLC is induced by adding the extra pure imaginary and odd-parity hopping integral  $\delta t^C = \pm i\eta$ , where  $\eta$  is a real number [37, 42, 43].  $\delta t^C$  is the symmetry breaking in the self-energy with TRS breaking, which appears due to the coexistence of the strong electron correlation and the geometrical frustration in kagome metals [34]. Figure 2 (a) shows the triple- $\mathbf{Q}$  cLC state derived from the density-wave (DW) equation [44–47] in the previous theoretical study [34]. In the triple- $\mathbf{Q}$  cLC order, the unit-cell is extended to  $2 \times 2$  that includes 12 sites. In Fig. 2 (a), the arrow from site  $j$  to site  $i$  represents  $\delta t_{i,j}^C = +i\eta$ , as shown in Fig. 2 (b). We note that  $\delta t_{i,j}^C = -\delta t_{j,i}^C$ . Here,

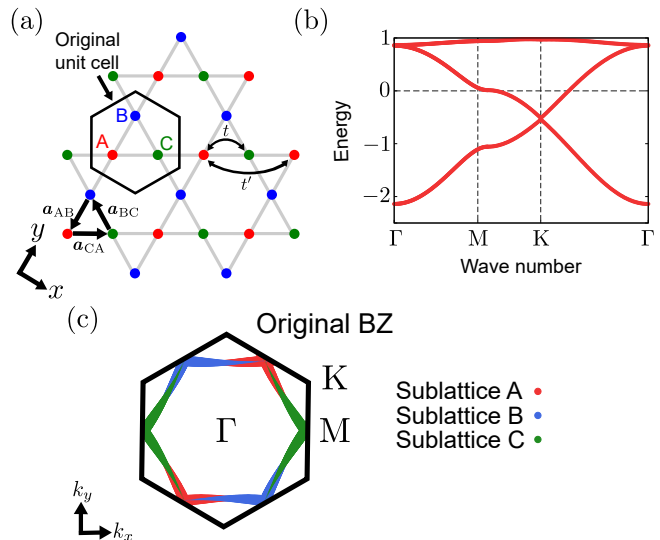


FIG. 1: (a) Kagome-lattice tight-binding model. The unit-cell is composed of the sublattices A, B, and C.  $2\mathbf{a}_{AB}$ ,  $2\mathbf{a}_{BC}$  give the three primitive vectors.  $\mathbf{a}_{CA} = -\mathbf{a}_{AB} - \mathbf{a}_{BC}$  (b) Band structure and (c) Fermi surface in the original Brillouin zone (BZ) at  $n = n_{\text{vHS}} = 2.55$ . Here, red, blue, and green colors represent the weight of the sublattices A, B, and C, respectively.

we assume that  $(i, j)$  is a nearest-neighbor bond for simplicity. Then,  $|\delta t_{i,j}^C|$  is equal to  $\eta$  for all the nearest bonds [34]. This cLC order corresponds to an odd-parity for a site exchange operation. For more detailed explanation of the cLC order in kagome metals, see Refs. [34, 35]. Ref. [35] points out that the current  $J_{i,j}$  is not proportional to  $\delta t_{i,j}^C$ , and three different  $|J_{i,j}|$  appear even when  $|\delta t_{i,j}^C|$  is same for all nearest-neighbor bonds. In Fig. 2 (a), the green (brown) circular arrows correspond to the triangular (hexagonal) current loops. In each circular arrow, all three or six arrows have the same chirality. Imp 1 (Imp 2) is the impurity site inserted on a triangular (hexagonal) loop. Importantly, the electronic states are unchanged if Imp 1 (Imp 2) occupies distinct positions of the triangular (hexagonal) loop, if one rotates the whole system appropriately. Because the number of the triangular loops is double of that of the hexagonal loops, a randomly introduced impurity belongs to Imp 1 or Imp 2 with the same probability (50 %).

To study the impurity effect in the cLC order, we construct the giant unit-cell model, where the 12 site extended unit-cell is arranged by  $M_x \times M_y$  and introduce single impurity potential  $I$  at one of the A sites.  $M_x$  and  $M_y$  are integers and we set up to  $M_x = M_y = 5$ , where the total site number is  $N = 12M_xM_y = 300$ . Then, the corresponding impurity density is  $n_{\text{imp}} = 0.33\%$ . We rigorously calculate the spatial distribution of the electronic states around the impurity without any approximation. (For example, the position of the impurity is averaged in the  $T$ -matrix approximation.) Figure 2 (a) shows the case of  $N = 48$  with  $M_x = M_y = 2$ , which corresponds

to  $n_{\text{imp}} = 2.08\%$ .

We consider the Hamiltonian

$$H = \sum_{\mathbf{k}, i, j, \sigma}^{\text{fBZ}} h_{i,j}(\mathbf{k}) c_{\mathbf{k}, i, \sigma}^\dagger c_{\mathbf{k}, j, \sigma} + \sum_{\mathbf{k}, \sigma}^{\text{fBZ}} I c_{\mathbf{k}, a, \sigma}^\dagger c_{\mathbf{k}, a, \sigma}, \quad (1)$$

where  $c_{\mathbf{k}, i, \sigma}$  ( $c_{\mathbf{k}, i, \sigma}^\dagger$ ) is an annihilation (creation) operator of an electron for the site  $i$  ( $i = 1-N$ ), the wave vector  $\mathbf{k}$ , and the spin  $\sigma$ . In Eq. (1), the  $\mathbf{k}$ -summation is taken inside the folded Brillouin zone (fBZ), whose size is  $1/4M_xM_y$  of the original BZ in Fig. 1 (c). In the first term,  $h_{i,j}(\mathbf{k})$  is the Fourier transformation of the hopping integral  $t_{i,j} = t_{i,j}^0 + \delta t_{i,j}^C$ . Here,  $t_{i,j}^0$  denotes the original hopping integral of the kagome lattice model, and  $\delta t_{i,j}^C$  is the modulation of the hopping integral by the cLC order. In the second term,  $I$  represents the impurity potential, and we put  $I = 100$  eV in the numerical study. This unitary limit impurity corresponds to a vacancy defect.  $a$  is the impurity site. We set the number of  $\mathbf{k}$  meshes  $N_{\mathbf{k}} = 512 \times 512$  in the fBZ in the numerical study. Then, we analyze the model with  $N$  periodically arranged  $N$ -site unit cells. That is, the number of sites included in the numerical study is  $N \times N_{\mathbf{k}}$ .

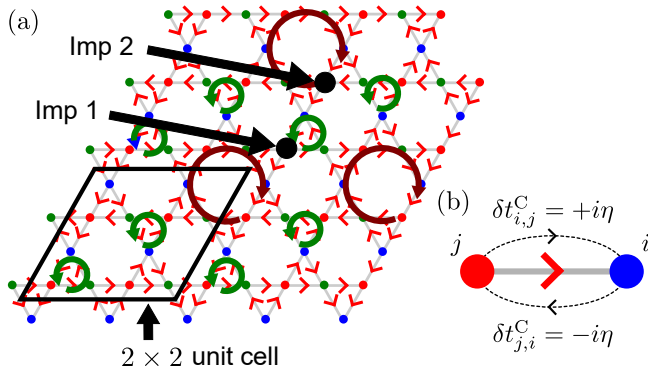


FIG. 2: (a) Giant unit-cell model for  $N = 48$  with  $M_x = M_y = 2$ , which corresponds to  $n_{\text{imp}} = 2.08\%$ . The unit-cell is extended to  $2 \times 2$  including 12 sites. The red arrows depict the triple- $Q$  cLC order. The black points represent the position of an introduced impurity. The impurity is introduced on a triangular (hexagonal) current loop in the Imp 1 (Imp 2) case. (b) Pure imaginary and odd-parity modulation of the hopping integral that induces the cLC.

### III. FORMALISM

To study the impurity effect, we calculate the current distribution in real space  $J_{i,j}$ , the uniform orbital magnetization  $M_{\text{orb}}$ , and the anomalous Hall conductivity  $\sigma_{xy}$ . First, we introduce the Green's function in real space,

$$G_{i,j}^\sigma(\mathbf{k}, \tau) = - \left\langle T \left[ c_{\mathbf{k}, i, \sigma} c_{\mathbf{k}, j, \sigma}^\dagger(\tau) \right] \right\rangle \quad (2)$$

to calculate the current distribution. Here,  $c_{\mathbf{k}, i, \sigma}(\tau) = e^{H\tau} c_{\mathbf{k}, i, \sigma} e^{-H\tau}$  is a Heisenberg operator for  $c_{\mathbf{k}, i, \sigma}$ . By

using Eq. (2), the current from site  $j$  to site  $i$ ,  $J_{i,j}$ , is given by [35]

$$J_{i,j} = i (t_{i,j} g_{j,i} - t_{j,i} g_{i,j}), \quad (3)$$

where  $g_{i,j}$  is defined as  $g_{i,j} = \lim_{\tau \rightarrow +0} \sum_{\sigma} G_{i,j}^\sigma(\tau)$ . Here, we set the charge of an electron  $-e$  as  $-1$ . Next, the orbital magnetization  $M_{\text{orb}}$  per site can be calculated by [48, 49]

$$M_{\text{orb}} = \frac{1}{\pi N_{\mathbf{k}} N} \sum_{n, \mathbf{k}}^{\text{fBZ}} \left[ m_{n, \mathbf{k}} f_{n, \mathbf{k}} - \Omega_{n, \mathbf{k}} T \ln \left( 1 + e^{-(\epsilon_{n, \mathbf{k}} - \mu)/T} \right) \right], \quad (4)$$

where

$$\begin{aligned} m_{n, \mathbf{k}} &= \frac{i}{2} \left[ \left\langle \nabla_{\mathbf{k}} u_{n, \mathbf{k}} \left| \times \left( \epsilon_{n, \mathbf{k}} - \hat{h}(\mathbf{k}) \right) \right| \nabla_{\mathbf{k}} u_{n, \mathbf{k}} \right\rangle_z \right. \\ &= \left. \frac{1}{2} \sum_{l \neq n} \text{Im} \left[ \frac{\left( v_{n, l, \mathbf{k}}^x \right)^* v_{n, l, \mathbf{k}}^y - v_{n, l, \mathbf{k}}^x \left( v_{n, l, \mathbf{k}}^y \right)^*}{\epsilon_{n, \mathbf{k}} - \epsilon_{l, \mathbf{k}}} \right] \right] \end{aligned} \quad (5)$$

and

$$\begin{aligned} \Omega_{n, \mathbf{k}} &= i \left[ \left\langle \nabla_{\mathbf{k}} u_{n, \mathbf{k}} \left| \times \left| \nabla_{\mathbf{k}} u_{n, \mathbf{k}} \right| \right\rangle_z \right. \\ &= \left. \sum_{l \neq n} \text{Im} \left[ \frac{\left( v_{n, l, \mathbf{k}}^x \right)^* v_{n, l, \mathbf{k}}^y - v_{n, l, \mathbf{k}}^x \left( v_{n, l, \mathbf{k}}^y \right)^*}{\left( \epsilon_{n, \mathbf{k}} - \epsilon_{l, \mathbf{k}} \right)^2} \right] \right] \end{aligned} \quad (6)$$

denote the orbital magnetic moment and the Berry curvature, respectively. Here, we use the relation

$$\langle u_{l, \mathbf{k}} \left| \nabla_{\mathbf{k}}^\mu \right| u_{m, \mathbf{k}} \rangle = \frac{v_{l, m, \mathbf{k}}^\mu}{\epsilon_{l, \mathbf{k}} - \epsilon_{m, \mathbf{k}}} \quad (7)$$

and  $v_{l, m, \mathbf{k}}^\mu = \langle u_{l, \mathbf{k}} \left| \nabla_{\mathbf{k}}^\mu \hat{h}(\mathbf{k}) \right| u_{m, \mathbf{k}} \rangle$  is the matrix element of the velocity operator for the wave vector  $\mathbf{k}$  in the band representation. In eq. (4), the first (second) term represents the contribution from the bulk (edge).  $f_{n, \mathbf{k}}$  is the Fermi distribution function,  $\epsilon_{n, \mathbf{k}}$  denotes the energy eigen value, and  $u_{n, \mathbf{k}}$  represents the Bloch wavefunction. The band indices  $n, l$  take values from 1 to  $N$ .

We note that  $M_{\text{orb}} \propto \eta^3$  without impurities as reported in Ref. [26] in the triple- $Q$  cLC order shown in Fig. 2 (a). The sign of  $M_{\text{orb}}$  is inverted when the sign of  $\eta$  is inverted. The finite  $M_{\text{orb}}$  originates from the incomplete cancelation of the magnetic flux, which is a natural consequence of the global TRS breaking in the triple- $Q$  cLC order. In other words, the time-reversal operation of the triple- $Q$  cLC order cannot be reproduced by its translational and rotational operations. On the other hand,  $M_{\text{orb}}$  vanishes in the single- $Q$  order, in which  $\eta \neq 0$  only in one direction, due to the global TRS.

Furthermore, we can evaluate the anomalous Hall conductivity  $\sigma_{xy}$  for  $T = 0$  by [50]

$$\sigma_{xy} = \sigma_{xy}^{\text{I}} + \sigma_{xy}^{\text{IIa}} + \sigma_{xy}^{\text{IIb}}. \quad (8)$$

Here,  $\sigma_{xy}^I$ ,  $\sigma_{xy}^{\text{IIa}}$ , and  $\sigma_{xy}^{\text{IIb}}$  are given by

$$\sigma_{xy}^I = -\frac{1}{\pi N_{\mathbf{k}} N} \sum_{l \neq m, \mathbf{k}}^{\text{fBZ}} \text{Im} \left[ v_{m,l,\mathbf{k}}^x v_{l,m,\mathbf{k}}^y \right] \times \text{Im} \left[ \frac{1}{(\epsilon_{l,\mathbf{k}} - \mu - i\gamma)(\epsilon_{m,\mathbf{k}} - \mu + i\gamma)} \right], \quad (9)$$

$$\sigma_{xy}^{\text{IIa}} = -\frac{1}{\pi N_{\mathbf{k}} N} \sum_{l \neq m, \mathbf{k}}^{\text{fBZ}} \text{Im} \left[ v_{m,l,\mathbf{k}}^x v_{l,m,\mathbf{k}}^y \right] \frac{1}{\epsilon_{l,\mathbf{k}} - \epsilon_{m,\mathbf{k}}} \times \text{Im} \left[ \frac{\epsilon_{l,\mathbf{k}} + \epsilon_{m,\mathbf{k}} - 2\mu - 2i\gamma}{(\epsilon_{l,\mathbf{k}} - \mu - i\gamma)(\epsilon_{m,\mathbf{k}} - \mu + i\gamma)} \right], \quad (10)$$

and

$$\sigma_{xy}^{\text{IIb}} = \frac{2}{\pi N_{\mathbf{k}} N} \sum_{l \neq m, \mathbf{k}}^{\text{fBZ}} \text{Im} \left[ v_{m,l,\mathbf{k}}^x v_{l,m,\mathbf{k}}^y \right] \frac{1}{(\epsilon_{l,\mathbf{k}} - \epsilon_{m,\mathbf{k}})^2} \times \text{Im} \left[ \ln \left( \frac{\epsilon_{l,\mathbf{k}} - \mu - i\gamma}{\epsilon_{m,\mathbf{k}} - \mu - i\gamma} \right) \right], \quad (11)$$

respectively. Here,  $\gamma (> 0)$  is the imaginary part of the self-energy.  $\sigma_{xy}^I$  and  $\sigma_{xy}^{\text{IIa}}$  are the contribution from the Fermi surface while  $\sigma_{xy}^{\text{IIb}}$  is the contribution from the Fermi sea by the Berry curvature:  $\sigma_{xy}^{\text{IIb}} \propto \sum_{n,\mathbf{k}} \Omega_{n,\mathbf{k}} f_{n,\mathbf{k}}$  for  $\gamma \rightarrow 0$  at  $T \rightarrow 0$ . We note that  $\sigma_{xy}$  also vanishes when the global TRS is preserved.

## IV. RESULT

### A. Impurity effect in the triple- $Q$ cLC

First, we calculate the current distribution  $J$  in the triple- $Q$  cLC state with an impurity for  $N = 192$  with  $M_x = M_y = 4$ , which corresponds to  $n_{\text{imp}} = 0.52\%$ . We note that when we introduce single impurity as a vacancy defect ( $I \approx \infty$ ), the effective electron filling at other sites is modified as

$$n_{\text{eff}} = \frac{N}{N-1} n, \quad (12)$$

where  $n$  is the original electron filling.

In Figs. 3 (a) and (b), the black point represents the impurity: Imp 1 in (a) and Imp 2 in (b). The blue dotted arrows denote the currents along a straight line through the impurity, which is expected to be suppressed near the impurity site. Other currents are shown by the gray arrows.

Figure 3 (c) [(d)] shows the obtained currents  $J_b$  along the  $b$ th bond from the impurity site on the blue dotted line in Fig. 3 (a) [(b)] for  $n_{\text{eff}} = 2.48$ . Here, the bond index  $b$  is shown in Figs. 3 (a) and (b). The

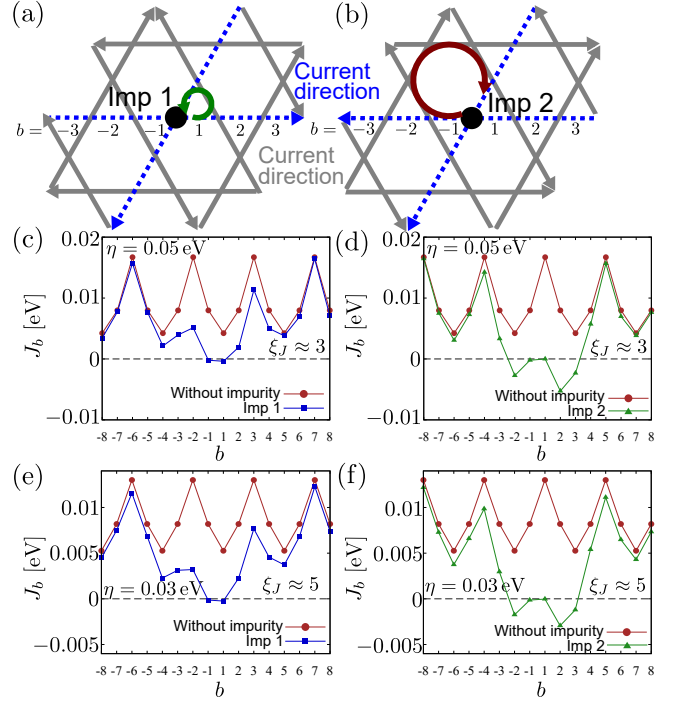


FIG. 3: (a) Schematic picture of the directions of  $\eta$  and the position of the impurity in the case of Imp 1 and (b) Imp 2. The black point is the impurity site. The blue and gray arrows represent the impurity and the current directions. (c) Obtained currents on the bonds along a straight line through the impurity in the Imp 1 case and (d) the Imp 2 case for  $\eta = 0.05$  eV,  $n_{\text{eff}} = 2.48$ . (e) Obtained currents on the bonds along a straight line through the impurity in the Imp 1 case and (f) the Imp 2 case for  $\eta = 0.03$  eV,  $n_{\text{eff}} = 2.48$ .  $J_b$  is the current along the  $b$ th bond. The red lines, the blue lines, and the green lines show the results without the impurity, the results of the Imp 1 case, and the Imp 2 case, respectively.

obtained currents on the two blue dotted lines are the same. These results indicate that currents near the impurity are drastically changed, while currents are almost unchanged by the impurity for  $|b| > \xi_J$ , where  $\xi_J$  is the current correlation length. As shown in Figs. 3 (c) and (d),  $\xi_J \approx 3$  for  $\eta = 0.05$  eV, while  $\xi_J$  increases to  $\approx 5$  for  $\eta = 0.03$  eV, as shown in Figs. 3 (e) and (f). The relation  $\xi_J \approx 0.15/\eta$  along the blue dotted line is numerically derived. This result reminds us of the BCS coherence length  $\xi_{\text{BCS}} = \pi v_F / \Delta_{\text{SC}}$ . Under the triple- $Q$  cLC order, the folded Fermi surfaces meet around the  $\Gamma$  point in the folded BZ. The band-hybridization gap  $\Delta_{\text{cLC}}$  due to the cLC order will be proportional to  $\eta$ . Therefore, the relation  $\xi_J \propto 1/\Delta_{\text{cLC}} \propto 1/\eta$  is naturally expected in Kagome metals.

Figure 4 represents the obtained  $\eta$  dependences of  $M_{\text{orb}}$  and  $\sigma_{xy}$  in the triple- $Q$  cLC order with an impurity for  $N = 300$  with  $M_x = M_y = 5$ , which corresponds to  $n_{\text{imp}} = 0.33\%$ . In the absence of the impurity,  $M_{\text{orb}} \propto \eta^3$ , as discussed in Ref. [26]. Interestingly, we find that  $M_{\text{orb}} \propto \eta^1$  in each case of Imp 1 or Imp 2, as shown in



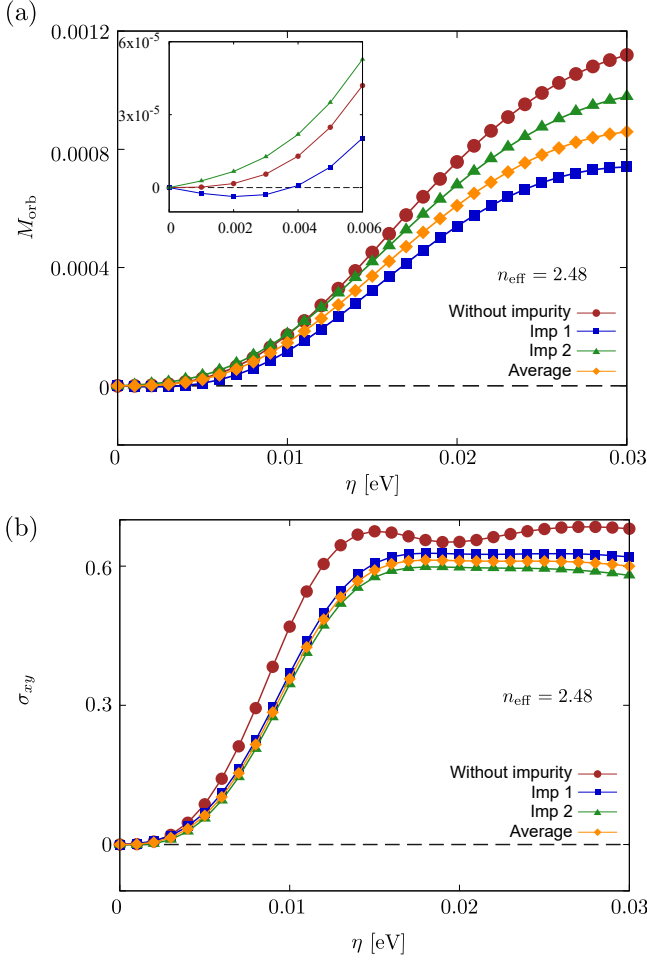


FIG. 4: (a) Obtained  $\eta$  dependences of  $M_{\text{orb}}$  and (b)  $\sigma_{xy}$  at  $n_{\text{eff}} = 2.48$ . The red lines, the blue lines, and the green lines represent the results without the impurity, the results of the Imp 1 case, and the Imp 2 case, respectively. The inset shows the obtained  $M_{\text{orb}}$  for  $0 \leq \eta \leq 0.006$ .

the inset of Fig. 4 (a). The orange lines represent the impurity-averaged result, in which the relation  $M_{\text{orb}} \propto \eta^3$  is recovered. We discover that both  $M_{\text{orb}}$  and  $\sigma_{xy}$  are drastically suppressed by dilute ( $= 0.33\%$ ) impurities. Overall, the impurity effect on  $M_{\text{orb}}$  is greater than that on  $\sigma_{xy}$ .

Figures 5 (a) and (b) show the effective electron filling  $n_{\text{eff}}$  dependences of  $M_{\text{orb}}$  and  $\sigma_{xy}$  under the condition of  $\eta = 0.01$  eV, respectively. The results for  $n_{\text{imp}} = 0.67, 1.00\%$  are obtained by linear extrapolation of the results for  $n_{\text{imp}} = 0$  and  $0.33\%$  since the reduction of  $M_{\text{orb}}$  and  $\sigma_{xy}$  are proportional to  $n_{\text{imp}}$  in the low impurity density region.  $|M_{\text{orb}}|$  has the main peak at  $n_{\text{eff}} = n_{\text{vHS}} = 2.55$ . In addition, two satellite peaks appear at  $n_{\text{eff}} = 2.46, 2.65$ , where the condition  $|\mu - \mu_{\text{vHS}}| \sim \max\{2\eta, T\}$  is fulfilled [26, 27]. Here,  $\mu_{\text{vHS}}$  is the chemical potential at  $n = n_{\text{vHS}} = 2.55$ . In the present case, we set  $\eta = T = 0.01$  eV, so that  $|\mu - \mu_{\text{vHS}}| \sim 0.02$  eV is satisfied at these fillings.

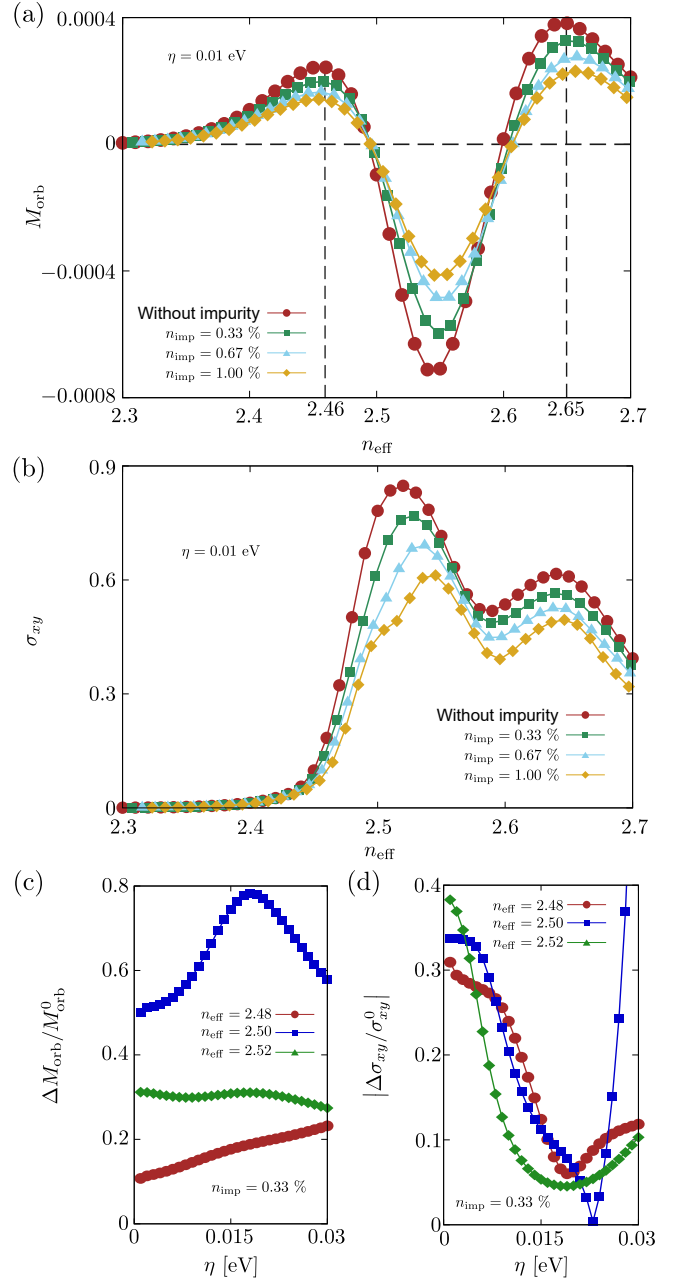


FIG. 5: (a) Obtained  $n_{\text{eff}}$  dependences of  $M_{\text{orb}}$  and (b)  $\sigma_{xy}$  for  $\eta = 0.01$  eV. The red lines, the green lines, the sky-blue lines, and the gold lines represent the results for  $n_{\text{imp}} = 0, 0.33, 0.67,$  and  $1.00\%$ , respectively. The results for  $n_{\text{imp}} = 0.67, 1.00\%$  are obtained by linear extrapolation of the results for  $n_{\text{imp}} = 0$  and  $0.33\%$ . (c) Obtained suppression ratio of  $M_{\text{orb}}$  and (d)  $\sigma_{xy}$ . The red lines, the blue lines, and the green lines represent the case of  $n_{\text{eff}} = 2.48, 2.50,$  and  $2.52$ , respectively.

Surprisingly, only  $\sim 1\%$  impurities reduce uniform  $|M_{\text{orb}}|$  by approximately  $40\%$  at arbitrary filling. To find the impurity effects in more detail, we show the suppression ratio  $R = -\Delta X/X^0$  at  $n_{\text{imp}} = 0.33\%$ , for  $X = M_{\text{orb}}$  in Fig. 5 (c) and  $X = \sigma_{xy}$  in Fig. 5 (d). Here,  $\Delta X$  denotes the change given by the impurity and  $X^0$  is the

quantity without the impurity. Both  $M_{\text{orb}}$  and  $\sigma_{xy}$  exhibit drastic suppression ratios for  $\eta < 0.01$ . Unexpectedly, the ratio  $R$  for  $M_{\text{orb}}$  is insensitive to  $\eta$ , in highly contrast to a naive expectation  $R \propto \xi_J^2$ . The obtained giant impurity effect of  $M_{\text{orb}}$  would originate from the non-local contribution from the itinerant circulation of electrons.

### B. Single- $Q$ cLC

Next, we study the impurity effect in the single- $Q$  cLC order. The single- $Q$  cLC order without the impurity is shown in Fig. 6 (a). In this case, the unit-cell is extended to  $2 \times 1$  that includes 6 sites. The single- $Q$  cLC breaks the local TRS, while  $M_{\text{orb}}$  and  $\sigma_{xy}$  vanish identically because the global TRS is preserved in the absence of the impurity.

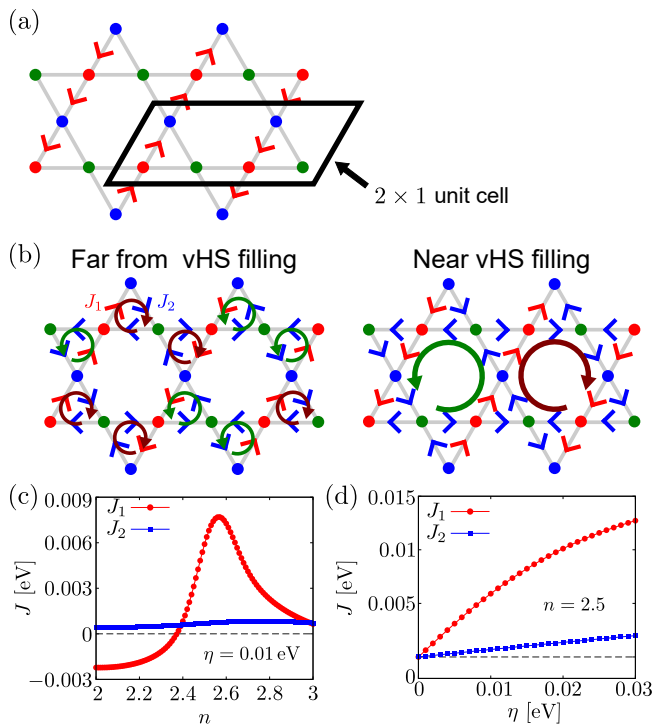


FIG. 6: (a) Kagome-lattice tight-binding model for the single- $Q$  cLC order. The unit-cell is extended to  $2 \times 1$  in the absence of the impurity. The arrows represent the directions of  $\eta$ . (b) Obtained current pattern when  $n$  is far from the vHS filling  $n_{\text{vHS}}$  (left) and  $n \approx n_{\text{vHS}}$  (right). The arrows depict the obtained current directions. The red arrows represent  $J_1$  that flows on the  $\eta \neq 0$  bonds. The blue arrows represent  $J_2$  that flows on the  $\eta = 0$  bonds. The green and brown circular arrows denote the loop currents with the opposite chirality. (c) Obtained  $n$  dependences of  $J_1$  and  $J_2$  for  $\eta = 0.01$  eV. (d)  $\eta$  dependences of  $J_1$  and  $J_2$  at  $n = 2.5$ .

Figure 6 (b) shows the schematic picture of the current pattern when  $n$  is far from the vHS filling  $n_{\text{vHS}}$  (left) and  $n \approx n_{\text{vHS}}$  (right). The numerical results are shown in Fig. 6 (c) for  $\eta = 0.01$  eV. In the single- $Q$  cLC order,  $|J_{i,j}| =$

$|J_1|$  for all  $\eta \neq 0$  bonds (red arrows) and  $|J_{i,j}| = |J_2|$  for all  $\eta = 0$  bonds (blue arrows). In Fig. 6 (c), the obtained  $J_1$  ( $J_2$ ) is shown by red (blue) lines, which is schematically shown by red (blue) arrows in Fig. 6 (b).  $J_1$  ( $J_2$ ) is the current on the bonds with  $\eta \neq 0$  ( $\eta = 0$ ). Interestingly,  $J_1$  exhibits the sign change as a function of  $n$  shown in Fig. 6 (c). Therefore, the triangular current loops are generated when  $n$  is far from  $n_{\text{vHS}}$ , while the hexagonal current loops are generated for  $n \approx n_{\text{vHS}}$ , as summarized in Fig. 6 (b). Both  $J_1$  and  $J_2$  are linear in  $\eta$ , as shown in Fig. 6 (d).

### C. Impurity effect in the single- $Q$ cLC

Next, we study the impurity effect in the single- $Q$  cLC order, in both cases of Imp 3 and Imp 4 shown in Fig. 7 (a). We first calculate the current distribution for  $N = 192$  with  $M_x = 4, M_y = 8$ , which corresponds to  $n_{\text{imp}} = 0.52\%$ . Figure 7 (b) shows the obtained current on the  $b$ th bond,  $J_b$ , in the case of Imp 3 that is inserted on the  $\eta \neq 0$  line. The bond indices  $b$  and  $b'$  are shown in Fig. 7 (a). In the case of Imp 3, the suppressed  $J_b$  near the impurity site recovers to the original value for  $|b| > \xi_J \approx 4$ . The derived  $\xi_J$  is similar to that obtained for the triple- $Q$  cLC order in Fig. 3. Figure 7 (c) shows the bond current in the case of Imp 4, which is introduced on the line with  $\eta = 0$ . In this case, the correlation length  $\xi_J$  is about 2.

Next, we calculate  $M_{\text{orb}}$  and  $\sigma_{xy}$  in the single- $Q$  cLC order with an impurity. In the case of Imp 3, both  $M_{\text{orb}}$  and  $\sigma_{xy}$  vanish because the global TRS is preserved. Therefore, we consider the Imp 4 case by setting  $N = 300$  with  $M_x = 5, M_y = 10$ , which corresponds to  $n_{\text{imp}} = 0.33\%$ . Figures 7 (d) and (e) represent the obtained  $\eta$  and  $n_{\text{eff}}$  dependences of  $M_{\text{orb}}$  and  $\sigma_{xy}$ , respectively. (The obtained  $M_{\text{orb}}$  and  $\sigma_{xy}$  are much smaller than those in the triple- $Q$  order in Figs. 4 and 5.) Interestingly, single nonmagnetic impurity gives rise to finite  $M_{\text{orb}}$  in the single- $Q$  cLC state, in which  $M_{\text{orb}}$  is absent without the impurity. However, the impurity-induced  $M_{\text{orb}}$  and  $\sigma_{xy}$  due to Imp 5 in Fig. 7 (a) are the inverses of those in Figs. 7 (d) and (e), because these two electronic states are converted by the TRS operation after the global shift by  $\pm 2\mathbf{a}_{\text{CA}}$ . Nonetheless, impurity-induced  $M_{\text{orb}}$  and  $\sigma_{xy}$  obtained in Figs. 7 (d) and (e) could be observed in microscopic measurements.

## V. SUMMARY

In this paper, we analyzed the giant unit-cell ( $N \leq 300$ ) kagome lattice model with single impurity potential to understand the impurity effects on the cLC electronic states accurately. The loop current is found to be strongly suppressed within the current correlation length  $\xi_J$  centered on the impurity site, where  $\xi_J$  is inversely proportional to the cLC order parameter  $\eta$ . For exam-

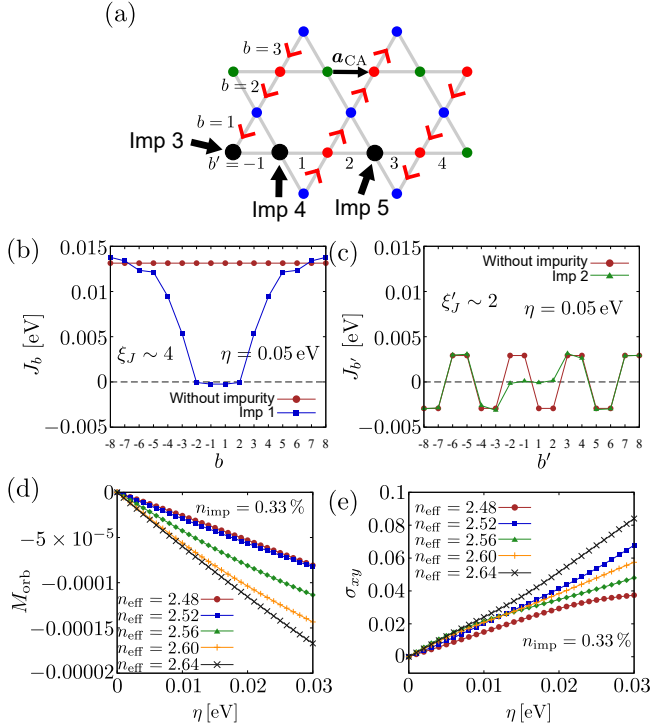


FIG. 7: (a) Kagome-lattice tight-binding model for the single- $\mathbf{Q}$  cLC order and the position of an introduced impurity in the Imp 3, the Imp 4, and the Imp 5 case. The red arrows represent the direction of  $\eta$ . (b) Obtained currents on the bonds along a straight line through the impurity in the Imp 3 case and (c) the Imp 4 case for  $\eta = 0.05$  eV and  $n_{\text{eff}} = 2.48$ . The red lines, the blue line, and the green line show the results without the impurity, the results of the Imp 3 case, and the Imp 4 case, respectively. (d) Obtained  $\eta$  dependences of  $M_{\text{orb}}$  and (e)  $\sigma_{xy}$  in the Imp 4 case under the condition of  $n_{\text{imp}} = 0.33\%$ .

ple, we obtain  $\xi_J \sim 3$  for  $\eta = 0.05$  and  $\xi_J \sim 5$  for  $\eta = 0.03$ . The relation  $\xi_J \approx 0.15/\eta$  is numerically derived. This result reminds us of the BCS coherence length  $\xi_{\text{BCS}} = \pi v_F/\Delta_{\text{SC}}$ . Under the triple- $\mathbf{Q}$  cLC order, the folded Fermi surfaces meet around the  $\Gamma$  point in the folded BZ. The band-hybridization gap  $\Delta_{\text{cLC}}$  due to the cLC order will be proportional to  $\eta$ . Therefore, the relation  $\xi_J \propto 1/\Delta_{\text{cLC}} \propto 1/\eta$  is naturally expected in kagome

metals.

In addition, we found that both the uniform orbital magnetization  $M_{\text{orb}}$  and the anomalous Hall conductivity  $\sigma_{xy}$  are drastically suppressed by dilute impurities. For both  $X = M_{\text{orb}}$  and  $\sigma_{xy}$ , the suppression ratio  $R = -\Delta X/X^0$  can exceed 50% by introducing just 1% impurities for  $\eta < 0.01$  eV; see Fig. 5 (c) for  $n_{\text{imp}} = 0.33$ . Unexpectedly, the ratio  $R$  is insensitive to  $\eta$  for  $X = M_{\text{orb}}$ , in highly contrast to a naive expectation  $R \propto \xi_J^2$ . This result indicates that  $M_{\text{orb}}$  is a non-local quantity whose length scale is much longer than  $\xi_J$ . The obtained giant impurity effects on  $M_{\text{orb}}$  and  $\sigma_{xy}$  in the  $2 \times 2$  cLC phase give a natural explanation why the cLC electronic states in kagome metals are extremely sensitive to the dilute impurities.

Recently, Asaba *et al.* discovered that the single- $\mathbf{Q}$  cLC order emerges above  $T_{\text{BO}} = 90$  K based on the magnetic torque measurement [9]. In the single- $\mathbf{Q}$  cLC state, both  $M_{\text{orb}}$  and  $\sigma_{xy}$  disappear because the global TRS is preserved. However, we find that an impurity in a nanoscale cluster model gives rise to finite  $M_{\text{orb}}$  and  $\sigma_{xy}$ , although they vanish by taking the average of the impurity sites. Interestingly, the single- $\mathbf{Q}$  cLC orders induce nontrivial loop current patterns, so the emerging characteristic magnetic fields could be observed experimentally.

In the present study, we assumed that the cLC order parameter  $\eta$  is constant for all the nearest bonds. However,  $\eta$  would be suppressed near the impurity site because the cLC order parameter is non  $s$ -wave, so it will be reduced by the impurity scattering without momentum conservation. In this respect, the drastic impurity effects on  $M_{\text{orb}}$  and  $\sigma_{xy}$  obtained here would be underestimated. This is an important future problem to study the impurity effect on  $\eta$  based on a microscopic theory.

## Acknowledgments

We are grateful to Y. Matsuda, T. Shibauchi, K. Hashimoto, T. Asaba and S. Suetsugu for very useful discussions. This study has been supported by Grants-in-Aid for Scientific Research from MEXT of Japan (JP24K00568, JP24K06938, JP23K03299, JP22K14003).

- [1] B. R. Ortiz, L. C. Gomes, J. R. Morey, M. Winiarski, M. Bordelon, J. S. Mangum, I. W. H. Oswald, J. A. Rodriguez-Rivera, J. R. Neilson, S. D. Wilson, E. Ertekin, T. M. McQueen, and E. S. Toberer, New kagome prototype materials: discovery of  $\text{KV}_3\text{Sb}_5$ ,  $\text{RbV}_3\text{Sb}_5$ , and  $\text{CsV}_3\text{Sb}_5$ , *Phys. Rev. Materials* **3**, 094407 (2019).
- [2] B. R. Ortiz, S. M. L. Teicher, Y. Hu, J. L. Zuo, P. M. Sarte, E. C. Schueller, A. M. M. Abeykoon, M. J. Krogstad, S. Rosenkranz, R. Osborn, R. Seshadri, L. Balents, J. He, and S. D. Wilson,  $\text{CsV}_3\text{Sb}_5$ : A  $Z_2$  Topological kagome metal with a superconducting ground state,

*Phys. Rev. Lett.* **125**, 247002 (2020).

- [3] Y.-X. Jiang, J.-X. Yin, M. M. Denner, N. Shumiya, B. R. Ortiz, G. Xu, Z. Guguchia, J. He, M. S. Hossain, X. Liu, J. Ruff, L. Kautzsch, S. S. Zhang, G. Chang, I. Belopolski, Q. Zhang, T. A. Cochran, D. Multer, M. Litskevich, Z.-J. Cheng, X. P. Yang, Z. Wang, R. Thomale, T. Neupert, S. D. Wilson, and M. Z. Hasan, Unconventional chiral charge order in kagome superconductor  $\text{KV}_3\text{Sb}_5$ , *Nat. Mater.* **20**, 1353 (2021).
- [4] H. Li, H. Zhao, B. R. Ortiz, T. Park, M. Ye, L. Balents, Z. Wang, S. D. Wilson, and I. Zeljkovic, Rotation symmetry

- breaking in the normal state of a kagome superconductor  $KV_3Sb_5$ , *Nat. Phys.* **18**, 265 (2022).
- [5] L. Nie, K. Sun, W. Ma, D. Song, L. Zheng, Z. Liang, P. Wu, F. Yu, J. Li, M. Shan, D. Zhao, S. Li, B. Kang, Z. Wu, Y. Zhou, K. Liu, Z. Xiang, J. Ying, Z. Wang, T. Wu, and X. Chen, Charge-density-wave-driven electronic nematicity in a kagome superconductor, *Nature* **604**, 59(2022).
- [6] T. Kato, Y. Li, T. Kawakami, M. Liu, K. Nakayama, Z. Wang, A. Moriya, K. Tanaka, T. Takahashi, Y. Yao, and T. Sato, Three-dimensional energy gap and origin of charge-density wave in kagome superconductor  $KV_3Sb_5$ , *Commun. Mater.* **3**, 30 (2022).
- [7] L. Nie, K. Sun, W. Ma, D. Song, L. Zheng, Z. Liang, P. Wu, F. Yu, J. Li, M. Shan, D. Zhao, S. Li, B. Kang, Z. Wu, Y. Zhou, K. Liu, Z. Xiang, J. Ying, Z. Wang, T. Wu, and X. Chen, Charge-density-wave-driven electronic nematicity in a kagome superconductor, *Nature* **604**, 59 (2022).
- [8] Y. Xu, Z. Ni, Y. Liu, B. R. Ortiz, Q. Deng, S. D. Wilson, B. Yan, L. Balents, and L. Wu, Three-state nematicity and magneto-optical Kerr effect in the charge density waves in kagome superconductors, *Nat. Phys.* **18**, 1470 (2022).
- [9] T. Asaba, A. Onishi, Y. Kageyama, T. Kiyosue, K. Ohtsuka, S. Suetsugu, Y. Kohsaka, T. Gaggli, Y. Kasahara, H. Murayama, K. Hashimoto, R. Tazai, H. Kontani, B. R. Ortiz, S. D. Wilson, Q. Li, H.-H. Wen, T. Shibauchi, and Y. Matsuda, Evidence for an odd-parity nematic phase above the charge-density-wave transition in a kagome metal, *Nat. Phys.* **20**, 40 (2024).
- [10] R. Tazai, Y. Yamakawa, S. Onari, and H. Kontani, Mechanism of exotic density-wave and beyond-Migdal unconventional superconductivity in kagome metal  $AV_3Sb_5$  ( $A=K, Rb, Cs$ ), *Sci. Adv.* **8**, eabl4108 (2022).
- [11] M. Roppongi, K. Ishihara, Y. Tanaka, K. Ogawa, K. Okada, S. Liu, K. Mukasa, Y. Mizukami, Y. Uwatoko, R. Grasset, M. Konczykowski, B. R. Ortiz, S. D. Wilson, K. Hashimoto, and T. Shibauchi, Bulk evidence of anisotropic  $s$ -wave pairing with no sign change in the kagome superconductor  $CsV_3Sb_5$ , *Nat Commun* **14**, 667 (2023).
- [12] W. Zhang, X. Liu, L. Wang, C. W. Tsang, Z. Wang, S. T. Lam, W. Wang, J. Xie, X. Zhou, Y. Zhao, S. Wang, J. Tallon, K. T. Lai, and S. K. Goh, Nodeless superconductivity in kagome metal  $CsV_3Sb_5$  with and without time reversal symmetry breaking, *Nano Lett.* **23**, 872 (2023).
- [13] L. Yu, C. Wang, Y. Zhang, M. Sander, S. Ni, Z. Lu, S. Ma, Z. Wang, Z. Zhao, H. Chen, K. Jiang, Y. Zhang, H. Yang, F. Zhou, X. Dong, S. L. Johnson, M. J. Graf, J. Hu, H.-J. Gao, and Z. Zhao, Evidence of a hidden flux phase in the topological kagome metal  $CsV_3Sb_5$ , [arXiv:2107.10714](https://arxiv.org/abs/2107.10714) (available at <https://arxiv.org/abs/2107.10714>).
- [14] C. Mielke III, D. Das, J.-X. Yin, H. Liu, R. Gupta, Y.-X. Jiang, M. Medarde, X. Wu, H. C. Lei, J. Chang, P. Dai, Q. Si, H. Miao, R. Thomale, T. Neupert, Y. Shi, R. Khasanov, M. Z. Hasan, H. Luetkens, and Z. Guguchia, Time-reversal symmetry-breaking charge order in a kagome superconductor, *Nature* **602**, 245 (2022).
- [15] R. Khasanov, D. Das, R. Gupta, C. Mielke III, M. Elenker, Q. Yin, Z. Tu, C. Gong, H. Lei, E. T. Ritz, R. M. Fernandes, T. Birol, Z. Guguchia, and H. Luetkens, Time-reversal symmetry broken by charge order in  $CsV_3Sb_5$ , *Phys. Rev. Res.* **4**, 023244 (2022).
- [16] Z. Guguchia, C. Mielke III, D. Das, R. Gupta, J.-X. Yin, H. Liu, Q. Yin, M. H. Christensen, Z. Tu, C. Gong, N. Shumiya, M. S. Hossain, T. Gamsakhurdashvili, M. Elenker, P. Dai, A. Amato, Y. Shi, H. C. Lei, R. M. Fernandes, M. Z. Hasan, H. Luetkens, and R. Khasanov, Tunable unconventional kagome superconductivity in charge ordered  $RbV_3Sb_5$  and  $KV_3Sb_5$ , *Nat. Commun.* **14**, 153 (2023).
- [17] J. Luo, Z. Zhao, Y. Z. Zhou, J. Yang, A. F. Fang, H. T. Yang, H. J. Gao, R. Zhou, and G.-q. Zheng, Possible star-of-David pattern charge density wave with additional modulation in the kagome superconductor  $CsV_3Sb_5$ , *npj Quantum Mater.* **7**, 30 (2022).
- [18] Y.-X. Jiang, J.-X. Yin, M. M. Denner, N. Shumiya, B. R. Ortiz, G. Xu, Z. Guguchia, J. He, M. S. Hossain, X. Liu, J. Ruff, L. Kautzsch, S. S. Zhang, G. Chang, I. Belopolski, Q. Zhang, T. A. Cochran, D. Multer, M. Litskevich, Z.-J. Cheng, X. P. Yang, Z. Wang, R. Thomale, T. Neupert, S. D. Wilson, and M. Z. Hasan, Unconventional chiral charge order in kagome superconductor  $KV_3Sb_5$ , *Nat. Mater.* **20**, 1353 (2021).
- [19] Y. Xu, Z. Ni, Y. Liu, B. R. Ortiz, Q. Deng, S. D. Wilson, B. Yan, L. Balents, and L. Wu, Three-state nematicity and magneto-optical Kerr effect in the charge density waves in kagome superconductors, *Nat. Phys.* **18**, 1470 (2022).
- [20] Y. Hu, S. Yamane, G. Mattoni, K. Yada, K. Obata, Y. Li, Y. Yao, Z. Wang, J. Wang, C. Farhang, J. Xia, Y. Maeno, S. Yonezawa, Time-reversal symmetry breaking in charge density wave of  $CsV_3Sb_5$  detected by polar Kerr effect, [arXiv:2208.08036](https://arxiv.org/abs/2208.08036) (available at <https://arxiv.org/abs/2208.08036>).
- [21] S.-Y. Yang, Y. Wang, B. R. Ortiz, D. Liu, J. Gayles, E. Derunova, R. Gonzalez-Hernandez, Sejkal, Y. Chen, S. S. P. Parkin, S. D. Wilson, E. S. Toberer, T. McQueen, and M. N. Ali, Giant, unconventional anomalous Hall effect in the metallic frustrated magnet candidate,  $KV_3Sb_5$ , *Sci. Adv.* **6**, eabb6003 (2020).
- [22] F. H. Yu, T. Wu, Z. Y. Wang, B. Lei, W. Z. Zhuo, J. J. Ying, and X. H. Chen, Concurrence of anomalous Hall effect and charge density wave in a superconducting topological kagome metal, *Phys. Rev. B* **104**, L041103 (2021).
- [23] Y. Wang, Z. Chen, Y. Nie, Y. Zhang, Q. Niu, G. Zheng, X. Zhu, W. Ning, and M. Tian, Nontrivial Fermi surface topology and large anomalous Hall effect in the kagome superconductor  $RbV_3Sb_5$ , *Phys. Rev. B* **108**, 035117 (2023).
- [24] C. Guo, C. Putzke, C. Konyzheva, S. Konyzheva, X. Huang, M. Gutierrez-Amigo, I. Errea, D. Chen, M. G. Vergniory, C. Felser, M. H. Fischer, T. Neupert, and P. J. W. Moll, Switchable chiral transport in charge-ordered kagome metal  $CsV_3Sb_5$ , *Nature* **611**, 461 (2022).
- [25] C. Guo, G. Wagner, C. Putzke, D. Chen, K. Wang, L. Zhang, M. Gutierrez-Amigo, I. Errea, M. G. Vergniory, C. Felser, M. H. Fischer, T. Neupert, and P. J. W. Moll, Correlated order at the tipping point in the kagome metal  $CsV_3Sb_5$ , *Nature Physics* **20**, 579 (2024).
- [26] R. Tazai, Y. Yamakawa, and H. Kontani, Drastic magnetic-field-induced chiral current order and emergent current-bond-field interplay in kagome metals, *Proc. Natl. Acad. of Sci. (PNAS)* **121**, e2303476121 (2024).
- [27] T. Park, M. Ye, and L. Balents, Electronic instabilities of kagome metals: Saddle points and Landau theory, *Phys.*



- Rev. B **104**, 035142 (2021).
- [28] Y.-P. Lin and R. M. Nandkishore, Complex charge density waves at Van Hove singularity on hexagonal lattices: Haldane-model phase diagram and potential realization in the kagome metals  $AV_3Sb_5$  ( $A=K, Rb, Cs$ ), Phys. Rev. B **104**, 045122 (2021).
- [29] M. L. Kiesel, C. Platt, and R. Thomale, Unconventional Fermi surface instabilities in the kagome Hubbard model, Phys. Rev. Lett. **110**, 126405 (2013).
- [30] W.-S. Wang, Z.-Z. Li, Y.-Y. Xiang, and Q.-H. Wang, Competing electronic orders on kagome lattices at van Hove filling, Phys. Rev. B **87**, 115135 (2013).
- [31] X. Wu, T. Schwemmer, T. Müller, A. Consiglio, G. Sangiovanni, D. D. Sante, Y. Iqbal, W. Hanke, A. P. Schnyder, M. M. Denner, M. H. Fischer, T. Neupert, and R. Thomale, Nature of Unconventional Pairing in the Kagome Superconductors  $AV_3Sb_5$  ( $A = K, Rb, Cs$ ), Phys. Rev. Lett. **127**, 177001 (2021).
- [32] M. M. Denner, R. Thomale, and T. Neupert, Analysis of Charge Order in the Kagome Metal  $AV_3Sb_5$  ( $A = K, Rb, Cs$ ), Phys. Rev. Lett. **127**, 217601 (2021).
- [33] M. H. Christensen, T. Biro, B. M. Andersen, and R. M. Fernandes, Loop currents in  $AV_3Sb_5$  kagome metals: Multipolar and toroidal magnetic order, Phys. Rev. B **106**, 144504 (2022).
- [34] R. Tazai, Y. Yamakawa, and H. Kontani, Charge-loop current order and  $Z_3$  nematicity mediated by bond order fluctuations in kagome metals, Nat. Commun. **14**, 7845 (2023).
- [35] K. Shimura, R. Tazai, Y. Yamakawa, S. Onari, and H. Kontani, Real-space loop current pattern in time-reversal-symmetry breaking phase in kagome metals, J. Phys. Soc. Jpn. **93**, 033704 (2024).
- [36] H. D. Scammell, J. Ingham, T. Li, and O. P. Sushkov, Chiral excitonic order from twofold van Hove singularities in kagome metals, Nat. Commun. **14**, 605 (2023).
- [37] F. Grandi, A. Consiglio, M. A. Sentef, R. Thomale, and D. M. Kennes, Theory of nematic charge orders in kagome metals, Phys. Rev. B **107**, 155131 (2023).
- [38] Y. Hu, X. Wu, B. R. Ortiz, S. Ju, X. Han, J. Ma, N. C. Plumb, M. Radovic, R. Thomale, S. D. Wilson, A. P. Schnyder, and M. Shi, Rich nature of Van Hove singularities in Kagome superconductor  $CsV_3Sb_5$ , Nat. Commun. **13**, 2220 (2022).
- [39] Y. Luo, S. Peng, S. M. L. Teicher, L. Huai, Y. Hu, B. R. Ortiz, Z. Wei, J. Shen, Z. Ou, B. Wang, Y. Miao, M. Guo, M. Shi, S. D. Wilson, and J.-F. He, Distinct band re-constructions in kagome superconductor  $CsV_3Sb_5$ , Phys. Rev. B **105**, L241111 (2022).
- [40] Z. Liu, N. Zhao, Q. Yin, C. Gong, Z. Tu, M. Li, W. Song, Z. Liu, D. Shen, Y. Huang, K. Liu, H. Lei, and S. Wang, Charge-Density-Wave-Induced Bands Renormalization and Energy Gaps in a Kagome Superconductor  $RbV_3Sb_5$ , Phys. Rev. X **11**, 041010 (2021).
- [41] K. Nakayama, Y. Li, T. Kato, M. Liu, Z. Wang, T. Takahashi, Y. Yao, and T. Sato, Carrier Injection and Manipulation of Charge-Density Wave in Kagome Superconductor  $CsV_3Sb_5$ , Phys. Rev. X **12**, 011001 (2022).
- [42] F. D. M. Haldane, Model for a Quantum Hall Effect without Landau Levels: Condensed-Matter Realization of the "Parity Anomaly", Phys. Rev. Lett. **61**, 2015 (1988).
- [43] C. M. Varma, Non-Fermi-liquid states and pairing instability of a general model of copper oxide metals. Phys. Rev. B **55**, 14554 (1997).
- [44] S. Onari, Y. Yamakawa, and H. Kontani, Sign-reversing orbital polarization in the nematic phase of FeSe due to the  $C_2$  symmetry breaking in the self-energy, Phys. Rev. Lett. **116**, 227001 (2016).
- [45] R. Tazai, Y. Yamakawa, and H. Kontani, Emergence of charge loop current in the geometrically frustrated Hubbard model: A functional renormalization group study, Phys. Rev. B **103**, L161112 (2021).
- [46] R. Tazai, S. Matsubara, Y. Yamakawa, S. Onari, and H. Kontani, Rigorous formalism for unconventional symmetry breaking in Fermi liquid theory and its application to nematicity in FeSe, Phys. Rev. B **107**, 035137 (2023).
- [47] J. Huang, R. Tazai, Y. Yamakawa, S. Onari, and H. Kontani, Low temperature phase transitions inside the CDW phase in the kagome metals  $AV_3Sb_5$  ( $A=Cs,Rb,K$ ): Significance of mixed-type Fermi surface electron correlations, Phys. Rev. B **109**, L041110 (2024).
- [48] D. Ceresoli, T. Thonhauser, D. Vanderbilt, and R. Resta, Orbital magnetization in crystalline solids: Multi-band insulators, Chern insulators, and metals, Phys. Rev. B **74**, 024408 (2006).
- [49] J. Shi, G. Vignale, D. Xiao, and Q. Niu, Quantum theory of orbital magnetization and its generalization to interacting systems, Phys. Rev. Lett. **99**, 197202 (2007).
- [50] T. Tanaka, H. Kontani, M. Naito, T. Naito, D. S. Hirashima, K. Yamada, and J. Inoue, Intrinsic spin Hall effect and orbital Hall effect in  $4d$  and  $5d$  transition metals, Phys. Rev. B **77**, 165117 (2008).